CARBON letters

Original Articles
Carbon Letters Vol. 24, 73-81 (2017)

Interconnected meso/microporous carbon derived from pumpkin seeds as an efficient electrode material for supercapacitors

Mayakrishnan Gopiraman[1], Somasundaram Saravanamoorthy[2], Seung-Hyun Kim[1] and Ill-Min Chung[1,♠]

[1]Department of Applied Bioscience, College of Life & Environment Science, Konkuk University, Seoul 05029, Korea
[2]Department of Chemistry, National Institute of Technology, Tiruchirappalli 620015, India

Article Info

Received 27 April 2017
Accepted 12 June 2017

♠Corresponding Author
E-mail: imcim@konkuk.ac.kr
Tel: +82-2-450-3730

Open Access

DOI: http://dx.doi.org/10.5714/CL.2017.24.73

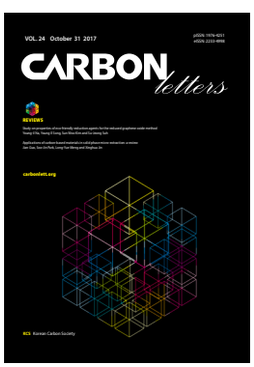

http://carbonlett.org

pISSN: 1976-4251
eISSN: 2233-4998

Abstract

Interconnected meso/microporous activated carbons were prepared from pumpkin seeds using a simple chemical activation method. The porous carbon materials were prepared at different temperatures (PS-600, PS-700, PS-800, and PS-900) and demonstrated huge surface areas (645–2029 $m^2\ g^{-1}$) with excellent pore volumes (0.27–1.30 $cm^3\ g^{-1}$). The well-condensed graphitic structure of the prepared activated carbon materials was confirmed by Raman and X-ray diffraction analyses. The presence of heteroatoms (O and N) in the carbon materials was confirmed by X-ray photoemission spectroscopy. High resolution transmission electron microscopic images and selected area diffraction patters further revealed the porous structure and amorphous nature of the prepared electrode materials. The resultant porous carbons (PS-600, PS-700, PS-800, and PS-900) were utilized as electrode material for supercapacitors. To our delight, the PS-900 demonstrated a maximum specific capacitance (Cs) of 303 F g^{-1} in 1.0 M H_2SO_4 at a scan rate of 5 mV. The electrochemical impedance spectra confirmed the poor electrical resistance of the electrode materials. Moreover, the stability of the PS-900 was found to be excellent (no significant change in the Cs even after 6000 cycles).

Key words: pumpkin seeds, activated carbon, electrode materials, supercapacitors, cycle stability

1. Introduction

Electrical double-layer capacitors (EDLCs), which are the most common type of supercapacitors, are widely used as advanced electrochemical power sources because they provide advantages of simple operation (via electrosorption of ions from an electrolyte onto high-surface area electrodes), rapid charge propagation dynamics, long cycle life performance (>100,000 cycles), a high charge/discharge rate and high power density [1,2]. As a consequence, EDLC supercapacitors are extensively used in various applications including electric vehicles, consumer electronics, electric pulse devices, as well as industrial power and energy management [3]. Several carbon-based electrode materials have been exploited in EDLCs, in particular, carbon nanotubes [4], carbon nanofibers [5] and graphene [6], due to their high surface area and excellent pore properties. For instance, single-layer-graphene has a theoretical specific surface area of 2630 $m^2\ g^{-1}$ and has demonstrated a specific capacitance of ~550 F g^{-1} [7].

However, the specific capacitance reported for pure graphene is found to be lower than the expected value, and this discrepancy is the result of the inherent tendency of the graphene layers to agglomerate face-to-face. Similarly, although carbon nanotubes possess a high specific surface area, their specific capacitances in most cases are very low, with values only in the range of 75–175 F g^{-1} and 40–100 F g^{-1} for aqueous and organic electrolytes,

respectively [5]. In addition, the cost of the carbon materials is moderately high.

Recently, porous carbon nanostructured materials derived from bio-mass have attracted increasing attention for use in supercapacitors because they exhibit tremendous specific surface area, interconnected porous structures, low cost, good electrical conductivity and excellent chemical stability [8,9]. So far, biomass derived porous activated carbons are the most widely commercialized supercapacitor electrode materials. Several bio-mass materials, including beer lees [10], coffee grounds [11], coffee endocarp [12], bamboo [13], pistachio shells [14], fir woods [15], walnut-shell [16] and so forth have been used as sources for the preparation of porous activated carbons. For instance, Nabais et al. [12] utilized coffee endocarps as a source of activated carbons. The obtained activated carbon had a specific surface area of 709 cm^2 g^{-1} and demonstrated good specific capacitance of 176 F g^{-1} at 1 mV s^{-1} in 1 M H_2SO_4. Hou et al. [17] derived N-doped 2D carbon nanosheets (NCN) from silk. The NCN showed a high level capacitance of 242 F g^{-1} with high cycling life stability which may be due to its unique 2D morphology, good porosity (2.28 m^3 g^{-1}) and high surface area (2494 m^2 g^{-1}). Similarly, 3D-honeycomb-like hierarchical structured carbon was fabricated from bacterial cellulose by Shan et al. [18]. Very recently, our research group utilized corn parts to obtain a 3D cheese-like carbon nanoarchitecture (CLCN) with huge specific surface area and pore construction [19]. The CLCN was used as a superior electrode material for supercapacitors. Despite these achievements, the search for highly suitable source material to prepare better electrode materials for supercapacitors continues.

According to previous findings [20,21], an ideal electrode material for supercapacitors should have at least four significant characteristics: 1) unique morphology (2D and 3D structures); 2) well-developed pore architecture to permit fast ion transportation on the surface of the electrode; 3) maximum surface area for better ion adsorption/desorption; and 4) better conductivity or low electric resistance for easy and efficient electron transport.

In the present study, pumpkin seeds (PS) were used to prepare a highly porous activated carbon for supercapacitors (PS-600, PS-700, PS-800, and PS-900). The resulting porous carbons were characterized by using X-ray diffraction (XRD), X-ray photoemission spectroscopy (XPS), high resolution transmission electron microscope-selected area diffraction (HRTEM-SEAD), Raman, energy dispersive spectroscope (EDS) and the Brunauer-Emmett-Teller (BET) method. After a complete characterization, the activated carbons were used as electrode materials for supercapacitors. Electrochemical impedance spectra were also taken for the electrode materials. The stability of the PS-900 was tested for 1000 cycles.

2. Experimental

2.1. Materials

PS were collected from a supermarket in South India. Nafion solution, hydrochloric acid (HCl), sodium hydroxide (NaOH), isopropanol and sulfuric acid (H_2SO_4) were purchased from Sigma Aldrich or Wako Pure Chemicals, Japan. Double distilled water was used to prepare the electrolyte solution. All chemicals were used as received.

2.2. Preparation of electrode materials

Initially, the fresh PS were washed with distilled water and oven-dried at 60°C for 24 h. Subsequently, the dried PS was pre-carbonized in a Muffle furnace under air atmosphere at 300°C for 1 h with a heating rate of 1°C/min. Then, the resultant pre-carbonized samples were mixed with NaOH (NaOH:pre-carbonized samples=2:1 ratio) and manually ground to make a homogeneous mixture. The above mixture was chemically activated at different temperatures (500, 600, 700, or 800°C). In a typical procedure, 1 g of pre-carbonized samples was mixed with 2 g of NaOH and then manually ground. The homogenous mixtures were carbonized at different temperatures (600–900°C) under N_2 flow for 1 h. Finally, the residues were washed with 1 M HCl solution and dried at 60°C for 24 h. The resultant activated carbons (designated by carbonization temperature as PS-600, PS-700, PS-800, and PS-900) were further studied.

2.3. Characterization

HRTEM and SAED images of the electrode materials (PS-600, PS-700, PS-800, and PS-900) were acquired on a JEOL JEM-2100F HRTEM with an accelerating voltage of 200 kV. The content of elements present in the electrode materials was determined using a scanning electron microscope-energy dispersive spectroscope (SEM-EDS; Hitachi 3000H SEM). The graphitic nature of the electrode materials was investigated by Raman spectroscopy using a Hololab 5000 (Kaiser Optical Systems Inc., USA). During the Raman analysis, the Ar laser functioned at 532 nm with a Kaiser holographic edge filter. XRD experiments were performed on the electrode materials at room temperature using a Rotaflex RTP300 (Rigaku Co., Japan) diffractometer. The instrument was operated at 40 kV and 200 mA with a scan speed of 2°/min. Nickel-filtered Cu K_α radiation ($10°<2\theta<60^o$) was used for the XRD measurements. XPS was recorded for the electrode materials using XPS, Kratos Axis-Ultra DLD (Kratos Analytical Ltd, Japan). The electrode samples were irradiated with a Mg Kα ray source for the XPS analysis. The BET method (BELSORP-max; BEL Japan, Inc.) was adopted to determine the specific surface area of the electrode materials. The electrochemical performance of the electrode materials was evaluated using a VersaSTAT-4 potentiostat (Ametek, USA) at a scan rate ranging from 5 to 100 mV s^{-1}.

2.4. Electrochemical measurements

Cyclic voltammetry (CV) measurements were performed in 1.0 M H_2SO_4 solutions and the sweep potential range was adjusted from –1.0 to 1.0 V (vs Ag/AgCl) in an electrochemical cell using a three-electrode system with platinum wire, Ag/AgCl, and the electrode materials (PS-600, PS-700, PS-800, and PS-900) as the counter, reference and working electrodes, respectively. This system was controlled by a VersaSTAT-4 potentiostat device.

First, the working electrode was prepared using the electrode

materials. In a typical preparation method, a mixture of 0.1–1.0 mg of the electrode materials, 20 μL Nafion solution (5 wt%) and 400 μL isopropanol was sonicated at room temperature for 1 h. Subsequently, 45 μL of the obtained slurry was poured on the active area of the glassy carbon electrode and dried at 80°C for 30 min. The galvanostatic charge–discharge experiment was carried out at 0.25 A g^{-1} over a voltage range of –0.4 to 0.6 V versus Ag/AgCl and the specific capacitance was calculated using the equation as follows:

$$C = I\Delta t/ m\Delta V \quad (1)$$

where I (A) is the discharge current, Δt (s) refers to the discharge time, and ΔV (V). ΔV is the potential window during the discharge process, and m (g) represents the weight of the electrode materials in the working electrode.

3. Results and Discussion

3.1. Characterization of the electrode materials

The electrode materials (PS-600, PS-700, PS-800, and PS-900) were prepared using pumpkin seeds (PS). First, the PS were washed with distilled water and oven-dried. Then, the dried PS was pre-carbonized in a Muffle furnace under air atmosphere at 300°C. The resulting pre-carbonized samples were mixed with NaOH and then manually ground to make a homogeneous mixture. Next, the mixture was activated under inert atmosphere at different temperatures (500, 600, 700, or 800°C). The resultant porous carbons (PS-600, PS-700, PS-800, and PS-900) were further studied.

The microstructures of the electrode materials were examined by HRTEM-SAED measurements. Fig. 1 shows the porous structure of PS-900. Mainly, two different types of carbon structures were noticed. The PS-900 has a very uniform microporous structure and no evident lattice fringe is found. The magnified HRTEM images clearly show the interconnected meso/micropores and channels. In addition, graphene-like carbon nanosheets with several wrinkles were also observed. The corresponding SAED pattern indicates the amorphous nature of PS-900 [22].

Raman spectra were recorded for all of the electrode materials (PS-600, PS-700, PS-800, and PS-900), and the data are presented in Fig. 2. All four samples exhibited two fundamental vibrations, the D band at 1349 cm^{-1} and G band at 1592 cm^{-1}. The strong G band represents the in-plane vibration of sp^2-hybridized carbon atoms in a graphite layer [11]. The strong D band is related to the sp^3 carbon atoms in the graphite layer, indicating the disordered crystalline structure of the carbon [15]. Generally, the G band in carbon materials appears at around 1985 cm^{-1}, however, in the present case, it was slightly upshifted (from 1985 to 1592 cm^{-1}) which confirms that the electrode materials have lots of micropores [23].

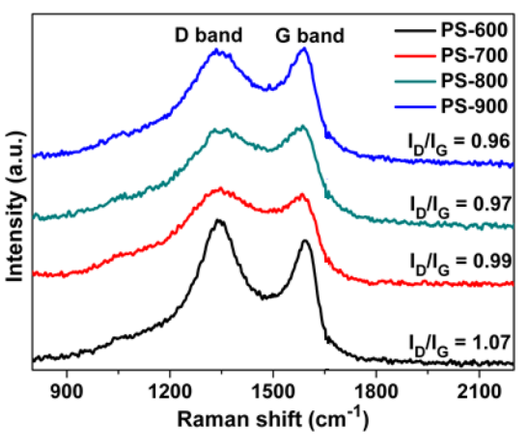

Fig. 2. Raman spectra of PS-600, PS-700, PS-800, and PS-900.

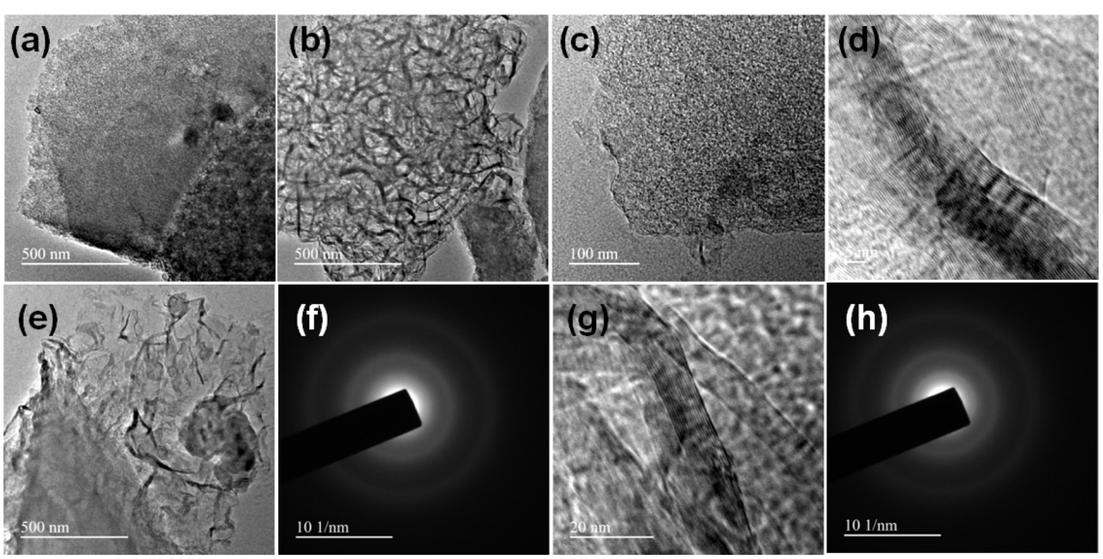

Fig. 1. (a-e, g) High resolution transmission electron microscope images and (f, h) selected area diffraction patterns of PS-900.

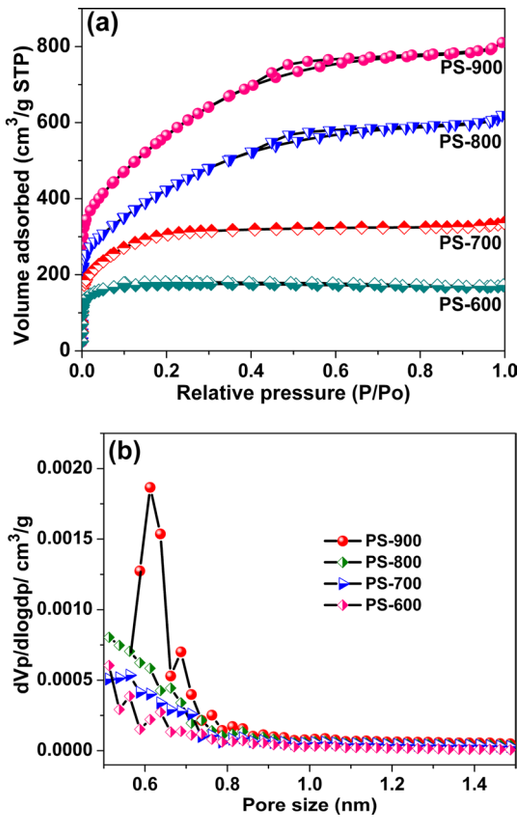

Fig. 3. (a) N_2 sorption isotherms and (b) the corresponding pore size distribution plots of PS-600, PS-700, PS-800, and PS-900.

The ratio of the relative intensity of the D band and G band (I_D/I_G) was calculated to understand the level of graphitization of the electrode materials. The I_D/I_G ratio is directly proportional to the amount of defect sites present in the carbon matrix. A higher value of I_D/I_G ratio shows a lower degree of graphitization in the electrode materials, which in porous carbon often results in poorer electrical conductivity [24].

Interestingly, in the present case, the I_D/I_G ratio gradually decreased when the activation temperature increased. A low I_D/I_G ratio of 0.96 was calculated for PS-900, whereas PS-600 showed a maximum I_D/I_G ratio of 1.07. The results indicate that the degree of graphitization in the electrode materials increases with increasing activation temperature. In comparison to PS-600, PS-700 and PS-800, PS-900 showed a low I_D/I_G ratio of 0.96 which indicates a better graphitized nature and, therefore, greatly improved electric conductivity.

Typical N_2 adsorption-desorption isotherms and the corresponding pore size distribution plots for PS-600, PS-700, PS-800 and PS-900 are provided in Fig. 3. The BET surface area, average pore size and pore volume of PS-600, PS-700, PS-800 and PS-900 are summarized in Table 1. For all the electrode samples, a significant amount of the N_2 uptake takes place at low relative pressure (P/P_0 <0.1), indicating that the electrode materials are typical microporous carbon [25]. Surprisingly, the N_2 adsorption-desorption isotherms of PS-800 and PS-900 show a gradual increase in relative pressure P/P_0 (upto 0.4), and a small hysteresis loop extending from P/P_0 0.4 to 0.6, indicating that the PS-800 and PS-900 materials have both micropores and mesopores [26].

According to previous findings, a small amount of mesopores (2–4 nm) in the electrode materials could provide low-resistance pathways for fast ion diffusion at high current densities, and enhance the ability of the microporous surface area to form electrochemical double-layers. The results in this study demonstrate that the electrode materials had a higher specific surface area with very good pore volume and average pore size (Table 1).

Like the degree of graphitization (see XRD and Raman results), the BET surface area of the electrode materials also increases with activation temperature. This phenomenon obviously has two main causes: 1) the volatilization of more unstable components at higher temperatures; and 2) high reaction activity between alkali and carbon under elevated temperature.

PS-900 demonstrated a maximum surface area of 2029 $m^2\ g^{-1}$ with a very good pore volume of 1.3 $cm^3\ g^{-1}$ and pore size of 2.5 nm; the surface area is very close to that of commercial activated carbon [27]. Moreover, the BET surface area of PS-900 is found to be high in comparison to other biomass derived activated carbons (see Table 2).

The influence of activation temperature and amount of NaOH on the surface area and porosity was also studied. The BET surface area of PS samples activated at 600°C (PS-600), 700°C (PS-700) and 800°C (PS-800) was determined to be 645, 1071 and 1517 $m^2\ g^{-1}$, while the pore volumes were 0.27, 0.53 and 0.91 $cm^3\ g^{-1}$, respectively (Table 2). Before NaOH activation, the electrode materials exhibited type-II isotherms (indicating non-porous materials), whereas, after activation at different temperatures (PS-600, PS-700, PS-800 and PS-900) they displayed

Table 1. Pore properties of electrode materials: elemental compositions of the electrode materials as determined by EDS and XPS analyses

Sample	Pore properties			EDS (at%)			XPS (at%)		
	S_{BET} ($m^2\ g^{-1}$)	V_{pore} ($cm^3\ g^{-1}$)	D_{aver} (nm)	C	N	O	C	N	O
PS-600	645	0.27	1.6	85.4	0.9	13.7	83.5	1.1	15.4
PS-700	1071	0.53	1.9	86.2	0.7	13.1	84.9	0.9	14.2
PS-800	1517	0.91	2.3	88.0	0.5	11.5	88.4	0.7	10.9
PS-900	2029	1.30	2.5	91.5	0.4	8.1	91.6	0.7	7.7

EDS, energy dispersive spectroscope; XPS, X-ray photoemission spectroscopy; BET, Brunauer-Emmett-Teller.

Table 2. Comparison of PS-900 to other biomass-derived activated carbons

S. no	Carbon source	S_{BET} ($m^2 g^{-1}$)	V_{pore} ($cm^3 g^{-1}$)/ D_{aver} (nm)	Cs ($F g^{-1}$) /scan rate	Electrolyte (mol L^{-1})	Stability (cycle/Cs)
1 [10]	Beer lees	3557	0.222/0.784	188/1 mA cm^{-2}	H_2SO_4, 0.1	-
2 [11]	Coffee grounds	1019	0.48/-	368/0.05 A g^{-1}	H_2SO_4, 1	10,000/350
3[a)]	Pumpkin seeds	2029	1.3/2.5	245/0.25 A g_{-1}	H_2SO_4, 1	1000/303
4 [19]	Corn fiber	2394	1.0954/1.8320	220/5 mV s^{-1}	H_2SO_4, 1	3000/225
5 [19]	Corn leafs	2793	1.2393/1.7750	280/5 mV s^{-1}	H_2SO_4, 1	3000/450
6 [12]	Coffee endocarp	709	0.34/1.15	176/1 mV s^{-1}	H_2SO_4, 1	-
7 [13]	Bamboo	1293	0.634/2.86	55/1 mA cm^{-2}	H_2SO_4, 1.5	-
8 [14]	Pistachio shells	1096	0.608/2.22	120/10 mV s^{-1}	H_2SO_4, 0.5	-
9 [15]	Fir woods	1064	0.607/2.28	180/10 mV s^{-1}	H_2SO_4, 0.5	-
10 [16]	Walnut-shell	2390	1.364/2.31	202.8/1 mA cm^{-2}	H_2SO_4, 3	1000/129

S, sample; BET, Brunauer-Emmett-Teller; Cs, specific capacitance.
[a)]Present study.

type-I sorption isotherms. The optimal ratio of C to NaOH was 1:2. Increasing the amount of NaOH collapses the pore construction due to the severe oxidation [28].

Overall, the high surface area, good pore volume and interconnections of the meso/micropores confirm that the electrode materials have better and faster ion transfer ability, by providing paths for the transportation and penetration of electrolyte ions. These characteristics confirm that it can be an ideal electrode material for supercapacitors. In addition, the NaOH activation method is an effective way to produce nano-scale pores in the carbon materials. The widely accepted mechanism for the activation of carbon using NaOH is as follows [29]: $6NaOH + 2C \rightarrow 2Na + 2Na_2CO_3 + 3H_2$, followed by decomposition of Na_2CO_3 and/or reaction of $Na/Na_2CO_3/CO_2$ with carbon.

Fig. 4 presents powder XRD patterns of the electrode materials (PS-600, PS-700, PS-800, and PS-900). Two broad diffraction bands with low intensity can be observed at 2θ=26° and 2θ=43° which are attributed to the (002) and (101) facets of the graphite-type carbon (JCPDS card no. 41-1487), respectively [14,15]. The low intensity and width of the diffraction peaks reveals that the electrode materials are amorphous in nature. Notably, the electrode material activated at 900°C (PS-900) showed a distinct graphite (002) peak with low intensity, which is in contrast to the other samples (PS-600, PS-700, and PS-800).

The results indicate that the electrode materials (particularly those prepared at elevated temperatures) consist of well-developed graphitic carbon with a higher degree of intralayer condensation [12-17]. The intensity of the (101) facet represents the higher integrity of the in-plane graphitic carbon skeleton. It was observed that the intensity of the (101) facet decreased gradually and had completely disappeared in PS-900. This phenomenon may be due to the increase in the degree of graphitization of the electrode materials as a result of alkali activation at high temperatures. Moreover, the high intensity in the low-angle region (2θ=15° to 5°) for PS-900

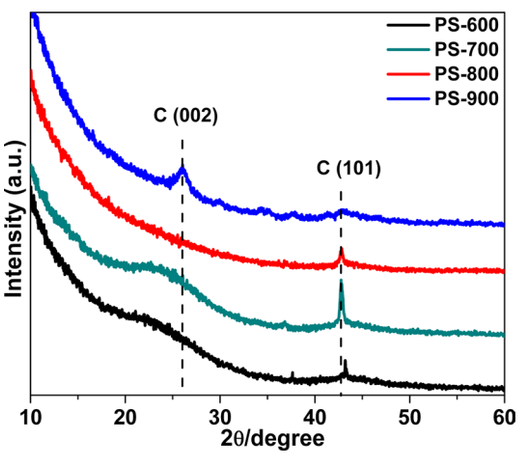

Fig. 4. X-ray diffraction patterns of PS-600, PS-700, PS-800, and PS-900.

may be due to the presence of a high-density of micropores in the carbon frame work [19].

The surface chemical properties of the present electrode materials were analyzed by XPS. Fig. 5 shows the XPS spectra of PS-600, PS-700, PS-800 and PS-900. The results obviously confirm the existence of two main elements, C (C 1s peak at ~284 eV), and O (O 1s peak at ~532 eV) in all four samples. In addition, a small peak corresponding to N (N 1s peak at ~401 eV) was also noticed.

In order to study the presence of oxygen functional groups in the electrode materials, curve fitting was performed on the C 1s and O 1s spectra of PS-900 using a Gaussian-Lorentzian peak shape. Prior to deconvolution, a Shirley baseline correction was done. The C 1s peak of PS-900 was deconvoluted into five peaks, which correspond to the C–C/C=C bonds (284.4 eV), C–O bonds (286 eV), C=O bonds (287.2 eV) and O–C=O bonds (289.6 eV) [30]. Moreover, the good intensity of the peak area

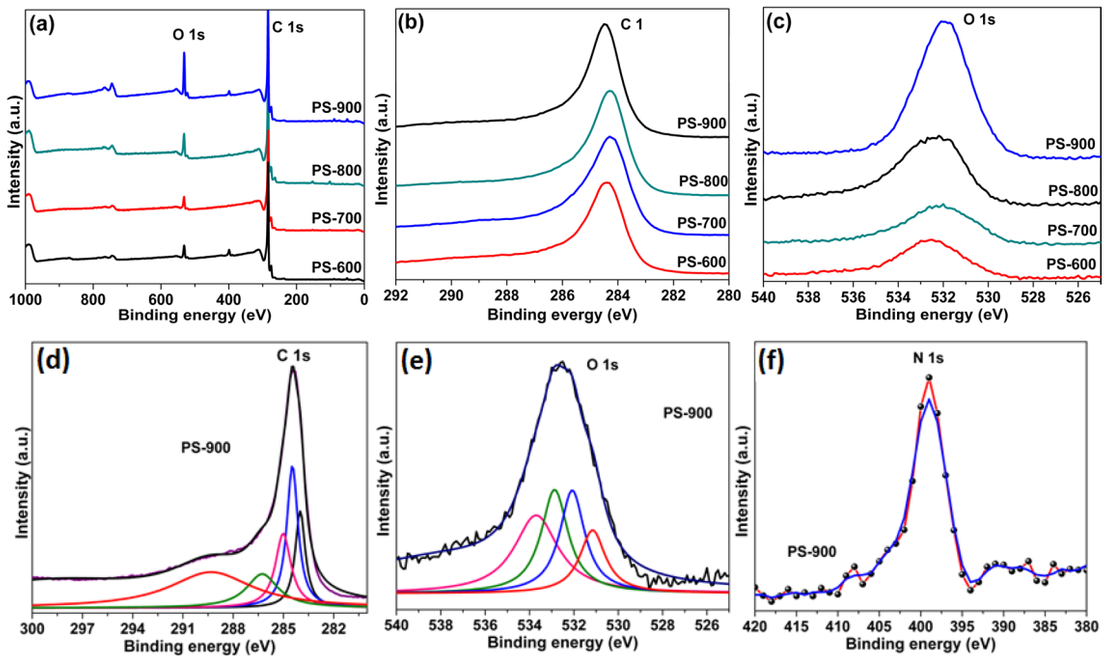

Fig. 5. X-ray photoemission spectroscopy (XPS) (a) survey spectra, (b) C 1s peaks, and (c) O 1s peaks of PS-600, PS-700, PS-800 and PS-900, and deconvoluted XPS (d) C 1s, (e) O 1s and (f) N 1s peaks of PS-900.

of the C–O bond reveals that the PS-900 has a large amount of oxygen on the surface.

Similarly, deconvolution of the O 1s peak of PS-900 resulted in four peaks located at 529.4, 530.5, 531.1 and 533.1 eV, which were assigned to the C=O, –COOH, C–OH and –C–O–C– bonds, respectively [30]. For all samples, the peaks at binding energies of ~400 eV confirmed the presence of N (possibly, pyridinic N, pyrrolic or pyridone N, and quaternary N) in the electrode materials [31]. It was noticed that the content of nitrogen and oxygen decreases with increasing calcination temperature. Generally, the presence of heteroatoms (O and N functional groups) in the carbon materials should induce additional faradaic pseudo-capacitance and provide better wettability between the electrode materials and electrolyte.

3.2. Electrochemical performance

CV and galvanostatic charge/discharge rates were used to test the electrochemical performance of the four electrode materials in 1 M H_2SO_4 solution. Fig. 6 depicts the typical CV curves of PS-600, PS-700, PS-800 and PS-900 at different scan rates, 5, 10, 20 and 50 mV s^{-1}. The PS-C before activation exhibited a very low specific capacitance, which may be due to its low surface area and low pore volume (data not shown). After chemical activation, the CV curves of PS-600, PS-700, PS-800 and PS-900 exhibited a quasi-rectangular voltammogram shape at low voltage scan rate, indicating good charge propagation within the electrodes, consistent with an outstanding electrode material for electrochemical double-layer capacitors.

In comparison to the CV curves of PS-600, PS-700 and PS-800, the CV curves of PS-900 showed a better rectangular shape. A rectangular shape indicates good charge propagation within the electrodes [18]. Even at a high scan rate (50 mV s^{-1}), PS-900 retained symmetric and rectangular-like CV curves. This might be due to the high surface area, large mesoporosity and low internal resistance of the electrode materials. Such features facilitate facile and fast electrolyte ion transport and shorten the diffusion distances from electrolyte to the inner micropore surface.

At a scan rate of 5 mV s^{-1}, the PS-600, PS-700, PS-800 and PS-900 samples showed a specific capacitance (Cs) of 101, 165, 213, and 303 F g^{-1}, respectively. The maximum Cs of 303 F g^{-1} was achieved by PS-900. The better Cs of PS-900 could be due to the following characteristics: 1) a huge BET surface area; 2) well-connected hierarchical micro/mesopores; 3) the presence of heteroatoms; and 4) good conductivity. In practice, PS-900's huge surface area (2029 m^2 g^{-1}) and good pore volume (1.3 cm^3 g^{-1}) would have assisted faster charge accumulation. The interconnected micro/mesopores also played a crucial role in achieving the high specific capacitance. The mesopores could also enhance the adsorption and transport of electrolytes.

Similarly, the micropores are responsible for diffusion of the electrolyte ions and faster charge accommodation. In addition, the large volume of interconnected micro/mesopores (1.3 cm^3 g^{-1}) would have facilitated a low-resistance pathway and provided good charge propagation and high current load capacity. In the present case, the reasonable amount of oxygen functionalities would have enhanced the wettability of PS-900 in aqueous electrolytes, which facilitates the infiltration of

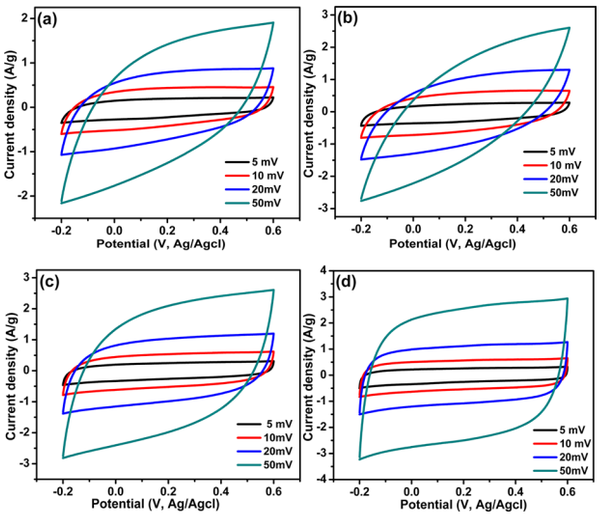

Fig. 6. Typical cyclic voltammograms of (a) PS-600, (b) PS-700, (c) PS-800 and (d) PS-900 at different scan rates (5, 10, 20 and 50 mV s^{-1}).

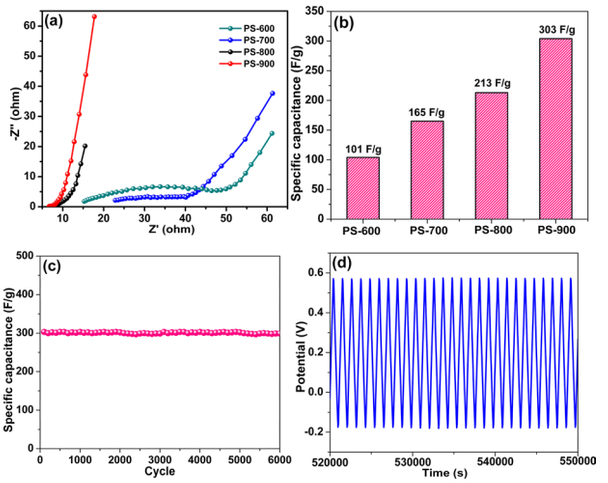

Fig. 7. (a) Nyquist plots and (b) specific capacitance of PS-600, PS-700, PS-800 and PS-900 at a scan rate of 5 mV s^{-1}; (c) cycling stability of PS-900, and (d) galvanostatic charge–discharge behavior of PS-900 supercapacitors.

electrolyte, allowing it to store energy in the deep inner voids.

The additional functional groups such as N and O would have also enhanced the surface utilization ratio of the active material. In addition, the presence of active nitrogen and/or oxygen heteroatoms might have assisted the high specific capacitance via the redox reactions of nitrogen functionalities on the surface of the electrode materials, e.g., >C=NH + $2e^-$ + $2H^+$ + >CH-NH_2 [30,31].

The measured specific capacitance of PS-900 was better or comparable to other reported biomass derived activated carbon electrode materials, including beer lees (188 F g^{-1} at scan rate of 1 mA cm^{-2}) [10], coffee grounds (368 F g^{-1} at 0.05 A g^{-1}) [11], corn fibers (220 F g^{-1} at 5 mV s^{-1}) [19], corn leaves (280 F g^{-1} at 5 mV s^{-1}) [19], coffee endocarp (176 F g^{-1} at 1 mV s^{-1}) [12], bamboo (55 F g^{-1} at 1 mA cm^{-2}) [13], pistachio shells (120 F g^{-1} at 10 mV s^{-1}) [14], fir wood (180 F g^{-1} at 10 mV s^{-1}) [15], and walnut-shells (202.8 F g^{-1} at 1 mA cm^{-2}) [16].

Generally, the microporous carbon materials that have numerous sub-nanometer-scale pores often show higher electrochemical performances in alkali ion-based electrolytes. We presumed that the present PS samples would show good electrochemical performance in alkali ion-based electrolytes as well.

3.3. Cycle stability

Fig. 7 shows the Nyquist plots and specific capacitance of PS-600, PS-700, PS-800 and PS-900. It was concluded that the electrical conductivity of the present electrode materials can be highly improved by increasing the activation temperature. The Nyquist plots of the electrode materials activated at 600°C and 700°C (PS-600 and PS-700) confirmed the poor conductive nature of the materials. Interestingly, the Nyquist plots of PS-800 and PS-900 indicated poor electrical resistance. Particularly, the Nyquist plots of PS-900 showed a smaller semicircle and nearly vertical lines in the electrochemical impedance spectroscopy curves at low frequency region. This is due to well-developed graphitic carbon with a higher degree of intralayer condensation.

The results reveal that the high specific capacitance of PS-900 could mainly be due to better electrolyte transport in the electrodes.

Excellent cycle stability was also confirmed for PS-900, even after 6000 cycles. PS-900 exhibited a maximum Cs of 299 F g^{-1} at the 6000th cycle. Moreover, the galvanostatic charge-discharge curves of PS-900 showed charge-discharge curves with isosceles triangular shapes (with no obvious IR drop), which indicates excellent capacitive behavior, low internal resistance and outstanding electrochemical reversibility for charge storage and release [31].

4. Conclusions

In conclusion, highly porous activated-carbons with good physicochemical properties were successfully prepared from pumpkin seeds (PS) by a simple NaOH activation method. At a scan rate of 5 mV s^{-1}, the PS-600, PS-700, PS-800 and PS-900 samples demonstrated a maximum specific capacitance (Cs) of 101, 165, 213, and 303 F g^{-1}, respectively. PS-900 even showed superior stability and higher capacitance after 6000 cycles, of 299 F g^{-1}. Overall, PS-900 offers advantages such as precursor stock availability, simple fabrication, unique morphology, excellent Cs and cycling stability, and for these reasons the electrode material could be useful for industrial applications.

Conflict of Interest

No potential conflict of interest relevant to this article was reported.

Acknowledgements

This study was supported by Konkuk University KU research professor program. This research was supported by Basic Science Research Program through the National Research Foundation of Korea (NRF) funded by the Ministry of Science, ICT and Future Planning (2015R1A2A1A15051532).

References

[1] Wang G, Zhang L, Zhang J. A review of electrode materials for electrochemical supercapacitors. Chem Soc Rev, **41**, 797 (2012). https://doi.org/10.1039/C1CS15060J.

[2] Guan C, Xia X, Meng N, Zeng Z, Cao X, Soci C, Zhang H, Fan HJ. Hollow core–shell nanostructure supercapacitor electrodes: gap matters. Energy Environ Sci, **5**, 9085 (2012). https://doi.org/10.1039/C2EE22815G.

[3] Kondrat S, Pérez CR, Presser V, Gogotsi Y, Kornyshev AA. Effect of pore size and its dispersity on the energy storage in nanoporous supercapacitors. Energy Environ Sci, **5**, 6474 (2012). https://doi.org/10.1039/C2EE03092F.

[4] Frackowiak E, Metenier K, Bertagna V, Beguin F. Supercapacitor electrodes from multiwalled carbon nanotubes. Appl Phys Lett, **77**, 2421 (2000). https://doi.org/10.1063/1.1290146.

[5] Wei K, Kim KO, Song KH, Kang CY, Lee JS, Gopiraman M, Kim IS. Nitrogen- and oxygen-containing porous ultrafine carbon nanofiber: a highly flexible electrode material for supercapacitor. J Mater Sci Technol, **33**, 424 (2017). https://doi.org/10.1016/j.jmst.2016.03.014.

[6] Yoo JJ, Balakrishnan K, Huang J, Meunier V, Sumpter BG, Srivastava A, Conway M, Reddy ALM, Yu J, Vajtai R, Ajayan PM. Ultrathin planar graphene supercapacitors. Nano Lett, **11**, 1423 (2011). https://doi.org/10.1021/nl200225j.

[7] Liu C, Yu Z, Neff D, Zhamu A, Jang BZ. Graphene-based supercapacitor with an ultrahigh energy density. Nano Lett, **10**, 4863 (2010). https://doi.org/10.1021/nl102661q.

[8] Zhang L, Zhang F, Yang X, Leng K, Huang Y, Chen Y. High-performance supercapacitor electrode materials prepared from various pollens. Small, **9**, 1342 (2013). https://doi.org/10.1002/smll.201202943.

[9] Yun YS, Cho SY, Shim J, Kim BH, Chang SJ, Baek SJ, Huh YS, Tak Y, Park YW, Park S, Jin HJ. Microporous carbon nanoplates from regenerated silk proteins for supercapacitors. Adv Mater, **25**, 1993 (2013). https://doi.org/10.1002/adma.201204692.

[10] Lee SG, Park KH, Shim WG, Balathanigaimani MS, Moon H. Performance of electrochemical double layer capacitors using highly porous activated carbons prepared from beer lees. J Ind Eng Chem, **17**, 450 (2011). https://doi.org/10.1016/j.jiec.2010.10.025.

[11] Yun YS, Park MH, Hong SJ, Lee ME, Park YW, Jin HJ. Hierarchically porous carbon nanosheets from waste coffee grounds for supercapacitors. ACS Appl Mater Interfaces, **7**, 3684 (2015). https://doi.org/10.1021/am5081919.

[12] Nabais JMV, Teixeira JG, Almeida I. Development of easy made low cost bindless monolithic electrodes from biomass with controlled properties to be used as electrochemical capacitors. Bioresour Technol, **102**, 2781 (2011). https://doi.org/10.1016/j.biortech.2010.11.083.

[13] Kim YJ, Lee BJ, Suezaki H, Chino T, Abe Y, Yanagiura T, Park KC, Endo M. Preparation and characterization of bamboo-based activated carbons as electrode materials for electric double layer capacitors. Carbon, **44**, 1592 (2006). https://doi.org/10.1016/j.carbon.2006.02.011.

[14] Xu J, Gao Q, Zhang Y, Tan Y, Tian W, Zhu L, Jiang L. Preparing two-dimensional microporous carbon from Pistachio nutshell with high areal capacitance as supercapacitor materials. Sci Rep, **4**, 5545 (2014). https://doi.org/10.1038/srep05545.

[15] Peng C, Yan XB, Wang RT, Lang JW, Ou YJ, Xue QJ. Promising activated carbons derived from waste tea-leaves and their application in high performance supercapacitors electrodes. Electrochim Acta, **87**, 401 (2013). https://doi.org/10.1016/j.electacta.2012.09.082.

[16] Choi WS, Shim WG, Ryu DW, Hwang MJ, Moon H. Effect of ball milling on electrochemical characteristics of walnut shell-based carbon electrodes for EDLCs. Microporous Mesoporous Mater, **155**, 274 (2012). https://doi.org/10.1016/j.micromeso.2012.01.006.

[17] Hou J, Cao C, Idrees F, Ma X. Hierarchical porous nitrogen-doped carbon nanosheets derived from silk for ultrahigh-capacity battery anodes and supercapacitors. ACS Nano, **9**, 2556 (2015). https://doi.org/10.1021/nn506394r.

[18] Shan D, Yang J, Liu W, Yan J, Fan Z. Biomass-derived three-dimensional honeycomb-like hierarchical structured carbon for ultrahigh energy density asymmetric supercapacitors. J Mater Chem A, **4**, 13589 (2016). https://doi.org/10.1039/C6TA05406D.

[19] Gopiraman M, Deng D, Kim BS, Chung IM, Kim IS. Three-dimensional cheese-like carbon nanoarchitecture with tremendous surface area and pore construction derived from corn as superior electrode materials for supercapacitors. Appl Surf Sci, **409**, 52 (2017). https://doi.org/10.1016/j.apsusc.2017.02.209.

[20] Xing W, Huang CC, Zhuo SP, Yuan X, Wang GQ, Hulicova-Jurcakova D, Yan ZF, Lu GQ. Hierarchical porous carbons with high performance for supercapacitor electrodes. Carbon, **47**, 1715 (2009). https://doi.org/10.1016/j.carbon.2009.02.024.

[21] Yu Z, Tetard L, Zhai L, Thomas J. Supercapacitor electrode materials: nanostructures from 0 to 3 dimensions. Energy Environ Sci, **8**, 702 (2015). https://doi.org/10.1039/C4EE03229B.

[22] Ning X, Zhong W, Li S, Wang Y, Yang W. High performance nitrogen-doped porous graphene/carbon frameworks for supercapacitors. J Mater Chem A, **2**, 8859 (2014). https://doi.org/10.1039/C4TA01038H.

[23] Korenblit Y, Rose M, Kockrick E, Borchardt L, Kvit A, Kaskel S, Yushin G. High-rate electrochemical capacitors based on ordered mesoporous silicon carbide-derived carbon. ACS Nano, **4**, 1337 (2010). https://doi.org/10.1021/nn901825y.

[24] Mao L, Zhang Y, Hu Y, Ho KH, Ke Q, Liu H, Hu Z, Zhao D, Wang J. Activation of sucrose-derived carbon spheres for high-performance supercapacitor electrodes. RSC Adv, **5**, 9307 (2015). https://doi.org/10.1039/c4ra11028e.

[25] Zhou M, Pu F, Wang Z, Guan S. Nitrogen-doped porous carbons through KOH activation with superior performance in supercapacitors. Carbon, **68**, 185 (2014). https://doi.org/10.1016/j.carbon.2013.10.079.

[26] Falco C, Marco-Lozar JP, Salinas-Torres D, Morallón E, Cazorla-Amorós D, Titirici MM, Lozano-Castelló D. Tailoring the porosity of chemically activated hydrothermal carbons: Influence of the precursor and hydrothermal carbonization temperature. Carbon, **62**, 346 (2013). https://doi.org/10.1016/j.carbon.2013.06.017.

[27] Dias JM, Alvim-Ferraz MC, Almeida MF, Rivera-Utrilla J, Sán-

chez-Polo M. Waste materials for activated carbon preparation and its use in aqueous-phase treatment: a review. J Environ Manage, **85**, 833 (2007). https://doi.org/10.1016/j.jenvman.2007.07.031.

[28] Elmouwahidi A, Zapata-Benabithe Z, Carrasco-Marín F, Moreno-Castilla C. Activated carbons from KOH-activation of argan (Argania spinosa) seed shells as supercapacitor electrodes. Bioresour Technol, **111**, 185 (2012). https://doi.org/10.1016/j.biortech.2012.02.010.

[29] Jun Y, Qian W, Wei T, Fan Z. Recent advances in design and fabrication of electrochemical supercapacitors with high energy densities. Adv Energy Mater, **4**, 1300816 (2014). https://doi.org/10.1002/aenm.201300816.

[30] Gopiraman M, Babu SG, Khatri Z, Kai W, Kim YA, Endo M, Karvembu R, Kim IS. Dry synthesis of easily tunable nano ruthenium supported on graphene: novel nanocatalysts for aerial oxidation of alcohols and transfer hydrogenation of ketones. J Phys Chem C, **117**, 23582 (2013). https://doi.org/10.1021/jp402978q.

[31] Gao F, Qu J, Zhao Z, Wang Z, Qiu J. Nitrogen-doped activated carbon derived from prawn shells for high-performance supercapacitors. Electrochim Acta, **190**, 1134 (2016). https://dx.doi.org/10.1016/j.electacta.2016.01.005.

[32] Yun YS, Lee S, Kim NR, Kang M, Leal C, Park KY, Kang K, Jin HJ. High and rapid alkali cation storage in ultramicroporous carbonaceous materials. J Power Sources, **313**, 142 (2016). https://dx.doi.org/10.1016/j.jpowsour.2016.02.068.